Available online at www.sciencedirect.com
ScienceDirect
Journal of Colloid and Interface Science 310 (2007) 27–34
JOURNAL OF Colloid and Interface Science
www.elsevier.com/locate/jcis

Using the Dugdale approximation to match a specific interaction in the adhesive contact of elastic objects

Zhijun Zheng, Jilin Yu *

CAS Key Laboratory of Mechanical Behavior and Design of Materials, University of Science and Technology of China, Hefei, Anhui 230027, PR China

Received 15 October 2006; accepted 17 January 2007

Available online 1 March 2007

Abstract

In the Maugis–Dugdale model of the adhesive contact of elastic spheres, the step cohesive stress σ_0 is arbitrarily chosen to be the theoretical stress σ_{th} to match that of the Lennard-Jones potential. An alternative and more reasonable model is proposed in this paper. The Maugis model is first extended to that of arbitrary axisymmetric elastic objects with an arbitrary surface adhesive interaction and then applied to the case of a power-law shape function and a step cohesive stress. A continuous transition is found in the extended Maugis–Dugdale model for an arbitrary shape index n. A three-dimensional Johnson–Greenwood adhesion map is constructed. A relation of the identical pull-off force at the rigid limit is required for the approximate and exact models. With this requirement, the stress σ_0 is found to be $k(n)\Delta\gamma/z_0$, where $k(n)$ is a coefficient, $\Delta\gamma$ the work of adhesion, and z_0 the equilibrium separation. Hence we have $\sigma_0 \doteq 0.588\Delta\gamma/z_0$, especially for $n = 2$. The prediction of the pull-off forces using this new value shows surprisingly better agreement with the Muller–Yushchenko–Derjaguin transition than that using $\sigma_{\text{th}} \doteq 1.026\Delta\gamma/z_0$, and this is true for other values of shape index n.
© 2007 Elsevier Inc. All rights reserved.

Keywords: Contact; Adhesion; Elastic; Power-law surface profile; Dugdale approximation; Pull-off force; Adhesion map; Lennard-Jones potential

1. Introduction

The behavior of frictionless adhesive contact between two elastic spheres has been well quantitatively analyzed by several continuum mechanics models. A comprehensive review is available in the monograph by Maugis [1]. The significant concepts and relations involved in these models have advanced the development of contact mechanics. The core of the contact mechanics problem is characterizing the consistent relation of the deformation and the interaction. The original treatments of this relation and the important contributions of the models are briefly reviewed below. We aim to provide a supplement to the Maugis model [2].

In 1971, a model based on the balance of the elastic, mechanical potential and surface energies was introduced by Johnson et al. [3], who treated the adhesive contact problem of elastic spheres similarly to that of a Griffith crack. This model is the first successful adhesive contact model, known as the Johnson–Kendall–Roberts (JKR) model. Its maximum adhesive force, i.e., the pull-off force $-P_c$, was immediately determined as $1.5\pi R\Delta\gamma$, with $R = (1/R_1 + 1/R_2)^{-1}$ being the equivalent radius of spheres and $\Delta\gamma$ being the work of adhesion. Later, assuming a mode I stress intensity factor at the edge of the contact, Maugis and Barquins [4] applied the fracture mechanics principle to the contact mechanics field and showed that the same result as that of the JKR model can be obtained by application of the Griffith relation $\mathcal{G} = \Delta\gamma$, where $\mathcal{G}$ is the strain energy release rate.

In 1975, an alternative model based on a "thermodynamic" method was introduced by Derjaguin et al. [5], who assumed that molecular attractions act on a ring-shaped zone around the contact but are unable to change the profile, which remains Hertzian. This model is known as the Derjaguin–Muller–Toporov (DMT) model. In this model the attraction force is $2\pi R\Delta\gamma$ at point contact but decreases rapidly to $\pi R\Delta\gamma$ with the increase of the approach, which was recognized to be incorrect [6,7]. Later, a direct "force" method was employed by Muller el al. [6] to attempt to correct the DMT model. The

* Corresponding author. Fax: +86 551 360 6459.
E-mail address: jlyu@ustc.edu.cn (J. Yu).

0021-9797/$ – see front matter © 2007 Elsevier Inc. All rights reserved.
doi:10.1016/j.jcis.2007.01.042

model based on this new method is usually called the improved DMT (IDMT) model. At this time, the attraction force increases from $2\pi R\Delta\gamma$ with the increase of the approach [7]. This new result was also concluded to be incorrect. In fact, the two methods do not satisfy the consistent relation of the deformation and the surface interaction. In further research, a constant attraction force $2\pi R\Delta\gamma$ during approach was revised by Maugis [2], who again applied the fracture concepts.

In the later 1970s, the apparent discrepancy between the DMT and JKR models with regard to the pull-off force caused a sharp debate, which was finally clarified by introducing a dimensionless parameter [8], known as the Tabor number, and verified with a Muller–Yushchenko–Derjaguin (MYD) transition [9,10]. The Tabor number is interpreted as the ratio of the elastic deformation resulting from adhesion to the effective range of surface forces,

$$\mu = \left(R\Delta\gamma^2/E^{*2}z_0^3\right)^{1/3}, \tag{1}$$

where z_0 is the equilibrium separation and $E^* = [(1-\nu_1^2)/E_1 + (1-\nu_2^2)/E_2]^{-1}$ is the reduced elastic modulus, with E_i and ν_i $(i = 1, 2)$ being Young's modulus and Poisson's ratio, respectively. The two models apply to the opposite extremes of the Tabor number. A continuous transition was first found by Muller et al. [9,10] with a full self-consistent model (FSCM) based on the Lennard-Jones potential. Another restricted self-consistent model (RSCM) was also employed to recover the JKR and DMT limits by Hughes and White [11,12]. Comprehensive behavior of the load–displacement curves can be quantitatively analyzed with these self-consistent models, which depend on a good numerical method of iterations [13–17].

In 1992, two independent relations, i.e., the condition of no singularity and the Griffith relation $\mathcal{G} = \Delta\gamma$, were employed by Maugis [2] to establish an analytical model based on the Dugdale approximation, i.e., step cohesive stress distribution. This model is named as the Maugis–Dugdale (M–D) model, in which self-consistent numerical calculations were avoided and the transition from DMT to JKR was again found, with a transition parameter defined as

$$\lambda = \sigma_0(9R/2\pi\Delta\gamma E^{*2})^{1/3}, \tag{2}$$

where σ_0 is the step cohesive stress in the Dugdale approximation. To match the Lennard-Jones potential, this stress was chosen to be the theoretical stress $\sigma_{\text{th}} \doteq 1.026\Delta\gamma/z_0$, which corresponds to $\lambda \doteq 1.157\mu$. However, this is somewhat arbitrary [18], but no other suggestion is presented in the literature. In 1998, some other approximations, such as the linear approximation, the parabolic approximation and the exponential interaction, were employed by Barthel [19], who concluded that the transition from DMT to JKR is barely sensitive to the nature of the interaction potential.

In 1997, Johnson and Greenwood [18] carried out an extensive comparison among these models. Based on the M–D model, they constructed an adhesion map with two coordinates, i.e., the transition parameter λ (or the Tabor number μ) and the dimensionless load $P/\pi R\Delta\gamma$, to indicate the appropriate use of the Hertz, Bradley, DMT, JKR, and M–D models.

These adhesive contact models can be extended to a more general surface shape, as shown by many researchers. For example, according to the shapes of atomic force microscope (AFM) tips [20,21], nano-indenters [22] and biological attachments [23], a power-law function is employed to describe the surface profile. In 1996, Carpick et al. [20,21] extended the JKR model to derive the analytical load function for an integer shape index. In 2001, Goryacheva and Makhovskaya [24] derived an extended M–D model for an even shape index. In 2004, Borodich and Galanov [22] extended the JKR and IDMT models for an arbitrary shape index.

In this paper we propose a new suggestion for the stress σ_0. With this aim, we first generalize an adhesive contact model for arbitrary axisymmetric elastic objects with an arbitrary surface adhesive interaction from the Maugis model. Then, an extended M–D model for power-law axisymmetric elastic objects is obtained and simplified under several limit conditions. Subsequently, the adhesive contact models are summarized in a three-dimensional adhesion map. Finally, the requirement of an identical rigid limit of the approximate and exact models is discussed and a more reasonable value of σ_0 is deduced for the sphere contact problem.

2. A generalized Maugis theory

We consider the frictionless adhesive contact between two axisymmetric elastic objects, which are schematically represented in Fig. 1. Under the assumption of small deformation, the distribution of the stress and deformation fields of the elastic objects can be regarded as that of an elastic half-space, which can be performed with a Hankel transform. All efforts are made to derive the load–displacement relation that characterizes the contact behaviors. It can be shown that the problem is equivalent to that of frictionless adhesive contact between a rigid axisymmetric indenter and an elastic half-space, which can be solved with a linear combination of solutions derived by Sneddon [25] and Lowengrub and Sneddon [26]. The surface shape is described by

$$f(\varrho) \equiv z(r) = z_1(r) + z_2(r), \quad \varrho = r/a, \tag{3}$$

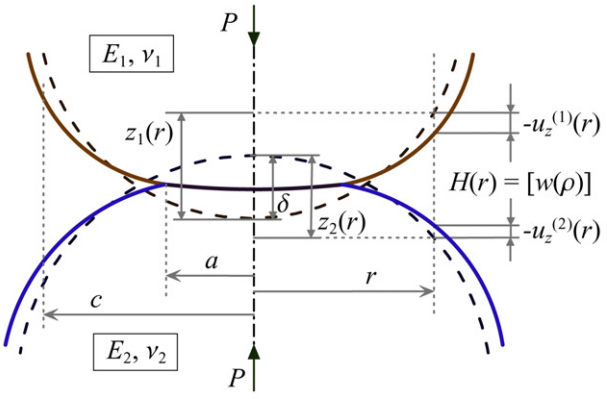

Fig. 1. Schematic representation of the deformation of two axisymmetric elastic objects, denoted as Solids 1 and 2. Solid curves represent the deformed surfaces and dashed curves represent the undeformed surfaces.

with $f'(\varrho) \geqslant 0$ and $f(0) = 0$, and the surface deformation and stress are equivalent by

$$\begin{cases} w(\varrho) \equiv u_z^{(1)}(r,0) + u_z^{(2)}(r,0), \\ \sigma(\varrho) \equiv \sigma_z^{(1)}(r,0) = \sigma_z^{(2)}(r,0), \\ \tau(\varrho) \equiv \tau_{rz}^{(1)}(r,0) = \tau_{rz}^{(2)}(r,0), \end{cases} \tag{4}$$

where r is the radius, a the contact radius, and superscripts (1) and (2) correspond to the two objects, respectively. The surface in contact is divided into three regions: an intimate contact region $r < a$, a cohesive region $a < r < c$, and a noninteraction region $r > c$. The mixed deformation and stress boundary conditions can be written as

$$\begin{cases} w(\varrho) = \delta - f(\varrho), & \varrho < 1, \\ \sigma(\varrho) = -p(\varrho), & \varrho > 1, \\ \tau(\varrho) = 0, & \varrho \geqslant 0, \end{cases} \tag{5}$$

where δ is the displacement and $p(\varrho)$ the surface pressure, with $p(\varrho) = 0$ at $\varrho > m = c/a$.

For the case of no adhesive interaction out of the contact area, i.e., $\sigma(\varrho) = 0$ at $\varrho > 1$, the Sneddon method [25] has solved the surface deformation and stress as

$$\begin{cases} w_{\mathrm{S}}(\varrho) = \int_0^1 \frac{\chi(t)}{\sqrt{\varrho^2 - t^2}}\,dt, & \varrho > 1, \\ \sigma_{\mathrm{S}}(\varrho) = -\frac{E^*}{2a}\left(\frac{\chi(1)}{\sqrt{1-\varrho^2}} - \int_\varrho^1 \frac{\chi'(t)}{\sqrt{t^2-\varrho^2}}\,dt\right), & \varrho < 1, \end{cases} \tag{6}$$

where $\chi(t)$ is defined as

$$\chi(t) = \frac{2}{\pi}\left(\delta - t\int_0^t \frac{f'(\ell)}{\sqrt{t^2-\ell^2}}\,d\ell\right). \tag{7}$$

And for the case of $w(\varrho) = 0$ at $\varrho < 1$, the Lowengrub and Sneddon method [26] shows that

$$\begin{cases} w_{\mathrm{LS}}(\varrho) = \frac{4}{\pi E^*}\int_1^\varrho \frac{g(t)}{\sqrt{\varrho^2-t^2}}\,dt, & \varrho > 1, \\ \sigma_{\mathrm{LS}}(\varrho) = \frac{2}{\pi a}\left(\frac{g(1)}{\sqrt{1-\varrho^2}} + \int_1^\infty \frac{g'(t)}{\sqrt{t^2-\varrho^2}}\,dt\right), & \varrho < 1, \end{cases} \tag{8}$$

where $g(t)$ is defined as

$$g(t) = a\int_t^\infty \frac{\ell p(\ell)}{\sqrt{\ell^2 - t^2}}\,d\ell. \tag{9}$$

Finally, the problem in the boundary conditions (5) can be directly solved by a linear combination of solutions in Eqs. (6) and (8):

$$\begin{cases} w(\varrho) = w_{\mathrm{S}}(\varrho) + w_{\mathrm{LS}}(\varrho), \\ \sigma(\varrho) = \sigma_{\mathrm{S}}(\varrho) + \sigma_{\mathrm{LS}}(\varrho). \end{cases} \tag{10}$$

Till now, the adhesive contact problem is not completely solved. Further physical conditions should be supplemented. The first relation is *the condition of no singularity* [1,2]:

$$\lim_{\varrho\to 1}\sqrt{2\pi a(1-\varrho)}\,\sigma(\varrho) = 0. \tag{11}$$

Substituting Eq. (10b) into this relation and associating Eq. (9), we have

$$\chi(1) = \frac{4}{\pi E^*}g(1) = \frac{4a}{\pi E^*}\int_1^\infty \frac{\ell p(\ell)}{\sqrt{\ell^2-1}}\,d\ell. \tag{12}$$

Then we derive

$$\sigma(\varrho) = -\frac{E^*}{\pi a}\int_\varrho^1\int_0^\varsigma \frac{(\ell f'(\ell))'}{\sqrt{(\varsigma^2-\varrho^2)(\varsigma^2-\ell^2)}}\,d\ell\,d\varsigma + \frac{2}{\pi}\int_1^\infty \frac{\ell p(\ell)}{\varrho^2-\ell^2}\sqrt{\frac{1-\varrho^2}{\ell^2-1}}\,d\ell, \quad \varrho < 1, \tag{13}$$

$$w(\varrho) = \frac{2\delta}{\pi}\operatorname{arccsc}\varrho - \frac{2}{\pi}\int_0^1 f'(\ell)\arctan\sqrt{\frac{1-\ell^2}{\varrho^2-1}}\,d\ell + \frac{4a}{\pi E^*}\int_1^\varrho\int_\varsigma^\infty \frac{\ell p(\ell)}{\sqrt{(\varrho^2-\varsigma^2)(\ell^2-\varsigma^2)}}\,d\ell\,d\varsigma, \quad \varrho > 1. \tag{14}$$

The second one is *the Griffith relation* [1,2],

$$\mathcal{G} \equiv -\int_1^m p(\varrho)\big([w(\varrho)]\big)'\,d\varrho = \Delta\gamma, \tag{15}$$

where the gap $[w(\varrho)]$ is given by

$$\big[w(\varrho)\big] = -\delta + f(\varrho) + w(\varrho). \tag{16}$$

The displacement can be determined from Eqs. (7) and (12):

$$\delta = \int_0^1 \frac{f'(\ell)}{\sqrt{1-\ell^2}}\,d\ell + \frac{\pi}{2}\chi(1) = \int_0^1 \frac{f'(\ell)}{\sqrt{1-\ell^2}}\,d\ell + \frac{2a}{E^*}\int_1^\infty \frac{\ell p(\ell)}{\sqrt{\ell^2-1}}\,d\ell. \tag{17}$$

Substituting Eqs. (5b) and (13) into

$$P = -2\pi a^2\int_0^\infty \sigma(\varrho)\varrho\,d\varrho, \tag{18}$$

we have the load

$$P = 2E^*a\int_0^1 \frac{\ell^2 f'(\ell)}{\sqrt{1-\ell^2}}\,d\ell + 4a^2\int_1^\infty \ell p(\ell)\left(\frac{1}{\sqrt{\ell^2-1}} + \operatorname{arcsec}\ell\right)d\ell. \tag{19}$$

Hence, the load–displacement relation of the generalized Maugis model is obtained in Eqs. (17) and (19) together with Eq. (15).

3. An extended Maugis–Dugdale theory

We have extended the Maugis model for the frictionless adhesive contact of arbitrary axisymmetric elastic objects with an arbitrary surface adhesive interaction. For simplicity, we consider the power-law shape function and the adhesive interaction

of the Dugdale approximation. The power-law shape function is described by

$$f(\varrho) = a^n \varrho^n / nQ, \tag{20}$$

where n and Q are two shape parameters. The shape index n is almost valid for all positive number, such as $n = 1$ for a cone, $n = 2$ for a sphere, and $n \to \infty$ for a flat punch. The dimension of Q is $\mathcal{L}^{n-1}$, with $\mathcal{L}$ being the length dimension. If $n = 1$, then $Q = \tan\varphi$, with φ being the semiangle; otherwise Q is usually denoted as R^{n-1}, with R being the equivalent radius. The Dugdale approximation is the approximation of the step cohesive pressure distribution,

$$p(\varrho) = -\sigma_0, \quad 1 < \varrho < m, \tag{21}$$

where σ_0 is a constant stress.

Substituting the surface shape function (20) and the surface adhesive interaction (21) into Eqs. (17) and (19), we have the displacement and load formulas,

$$\delta \equiv \delta_{\mathrm{H}} + \delta_{\mathrm{a}} = \tfrac{1}{2}\mathbf{B}\left(\tfrac{n}{2}, \tfrac{1}{2}\right) Q^{-1} a^n - \left(2\sigma_0 a / E^*\right)\sqrt{m^2 - 1}, \tag{22}$$

$$P \equiv P_{\mathrm{H}} + P_{\mathrm{a}} = \mathbf{B}\left(\tfrac{n}{2} + 1, \tfrac{1}{2}\right) E^* Q^{-1} a^{n+1} - 2\sigma_0 a^2 \left(m^2 \operatorname{arcsec} m + \sqrt{m^2 - 1}\right), \tag{23}$$

where $\mathbf{B}(\alpha, \beta)$ is the Euler beta function; subscripts "H" and "a" are referred to the corresponding contributions of the surface shape function and the surface adhesive interaction, respectively. The parameter m is determined from the Griffith relation (15), which is rewritten as

$$\frac{\sigma_0 a^n}{nQ}\left[m^n\left(1 - \mathbf{I}_{m^{-2}}\left(\tfrac{n+1}{2}, \tfrac{1}{2}\right)\right) - \tfrac{n}{\pi}\mathbf{B}\left(\tfrac{n}{2}, \tfrac{1}{2}\right)\operatorname{arcsec} m\right] + \frac{4\sigma_0^2 a}{\pi E^*}\left(\sqrt{m^2 - 1}\,\operatorname{arcsec} m + 1 - m\right) = \Delta\gamma, \tag{24}$$

where $\mathbf{I}_x(\alpha, \beta) \equiv \mathbf{B}_x(\alpha, \beta)/\mathbf{B}(\alpha, \beta)$ is the regularized beta function with $\mathbf{B}_x(\alpha, \beta)$ being the incomplete beta function. For given material properties (E^*, $\Delta\gamma$, and σ_0) and shape parameters (n and Q), the load–displacement relation is determined from Eqs. (22)–(24). For $n = 2$ and $Q = R$, these formulas reduce to those in the original M–D model [2], which have been extended for any positive even shape index by Goryacheva and Makhovskaya [24]. Now, the M–D model is extended for an arbitrary $n > 0$. For convenience, we denote this extended M–D model as "M–D–n," with n being the shape index.

We introduce the dimensionless parameters as follows:

$$\tilde{a} \equiv a/(Q^2 \Delta\gamma E^{*n-1})^{1/(2n-1)}, \tag{25}$$

$$\tilde{\delta} \equiv \delta/(Q \Delta\gamma^n E^{*n})^{1/(2n-1)}, \tag{26}$$

$$\tilde{P} \equiv P/\pi(Q^3 \Delta\gamma^{n+1} E^{*n-2})^{1/(2n-1)}, \tag{27}$$

$$\Lambda \equiv \sigma_0 (Q \Delta\gamma^{1-n} E^{*n})^{1/(2n-1)}. \tag{28}$$

For $n = 2$ and $Q = R$, a difference in the coefficients is noticed between our notations and those defined by Maugis [2], for example, $\lambda = (9/2\pi)^{1/3}\Lambda \doteq 1.127\Lambda$, but it does not cause any essential change. With our notations, the dimensionless load–displacement relation leads to

$$\tilde{\delta} \equiv \tilde{\delta}_{\mathrm{H}} + \tilde{\delta}_{\mathrm{a}} = \tfrac{1}{2}\mathbf{B}\left(\tfrac{n}{2}, \tfrac{1}{2}\right)\tilde{a}^n - 2\Lambda\tilde{a}\sqrt{m^2 - 1}, \tag{29}$$

$$\tilde{P} \equiv \tilde{P}_{\mathrm{H}} + \tilde{P}_{\mathrm{a}} = \tfrac{1}{\pi}\mathbf{B}\left(\tfrac{n}{2} + 1, \tfrac{1}{2}\right)\tilde{a}^{n+1} - \tfrac{2}{\pi}\Lambda\tilde{a}^2\left(m^2 \operatorname{arcsec} m + \sqrt{m^2 - 1}\right), \tag{30}$$

with the Griffith relation in dimensionless form,

$$\tfrac{1}{n}\Lambda\tilde{a}^n\left[m^n\left(1 - \mathbf{I}_{m^{-2}}\left(\tfrac{n+1}{2}, \tfrac{1}{2}\right)\right) - \tfrac{n}{\pi}\mathbf{B}\left(\tfrac{n}{2}, \tfrac{1}{2}\right)\operatorname{arcsec} m\right] + \tfrac{4}{\pi}\Lambda^2\tilde{a}\left(\sqrt{m^2 - 1}\,\operatorname{arcsec} m + 1 - m\right) = 1. \tag{31}$$

4. The transition from DMT-n to JKR-n

It is not difficult to solve the extended M–D model with a numerical calculation. For some limit conditions, it can even be simplified to a completely analytic form.

When the load is sufficiently high, the adhesive component may be neglected, i.e., $|P_{\mathrm{a}}/P| \ll 1$. In this case, one may have $\tilde{\delta} = \tilde{\delta}_{\mathrm{H}}$ and $\tilde{P} = \tilde{P}_{\mathrm{H}}$ in simplicity. This is an extended Hertz theory (denoted as Hertz-n) for power-law axisymmetric elastic objects.

When Λ is large, $m \to 1$ and Eq. (31) leads to

$$m^2 - 1 \simeq \pi/(2\Lambda^2\tilde{a}). \tag{32}$$

Then the load–displacement relation is simplified as

$$\tilde{\delta} \equiv \tilde{\delta}_{\mathrm{H}} + \tilde{\delta}_{\mathrm{a}} = \tfrac{1}{2}\mathbf{B}\left(\tfrac{n}{2}, \tfrac{1}{2}\right)\tilde{a}^n - \sqrt{2\pi\tilde{a}}, \tag{33}$$

$$\tilde{P} \equiv \tilde{P}_{\mathrm{H}} + \tilde{P}_{\mathrm{a}} = \tfrac{1}{\pi}\mathbf{B}\left(\tfrac{n}{2} + 1, \tfrac{1}{2}\right)\tilde{a}^{n+1} - \tfrac{2}{\pi}\sqrt{2\pi\tilde{a}^3}. \tag{34}$$

This is an extended JKR theory for an arbitrary $n > 0$, denoted as JKR-n. For $n = 2$ and $Q = R$, these formulas reduce to those by Johnson et al. [3]. For $n \to \infty$ and $Q = R^{n-1}$, these formulas reduce to those by Kendall [27]. For $n = 1$ and $Q = \tan\varphi$, these formulas reduce to those of Maugis and Barquins [28]. The load formula has also been presented by Carpick et al. [20,21] for any integer $n > 0$, and by Borodich and Galanov [22] for an arbitrary $n > 0$. Compared to the extended Hertz theory, an infinite stress at the edge of the contact is found, which corresponds to a mode I stress intensity factor $K_I = \sqrt{2\Delta\gamma E^*}$. The pull-off force can be obtained as

$$-\tilde{P}_{\mathrm{c}}^{\text{JKR-}n} = \frac{2(2n-1)}{(n+1)\sqrt{2\pi}}\left(\frac{3\sqrt{2\pi}}{n\mathbf{B}\left(\frac{n}{2}, \frac{1}{2}\right)}\right)^{3/(2n-1)}, \tag{35}$$

which has been presented by several researchers [22,23].

When Λ is small, $m \to \infty$, and Eq. (31) shows that

$$m \simeq (n/\Lambda)^{1/n}/\tilde{a}. \tag{36}$$

In this case, we have the dimensionless load–displacement relation as

$$\tilde{\delta} \equiv \tilde{\delta}_{\mathrm{H}} + \tilde{\delta}_{\mathrm{a}} = \tfrac{1}{2}\mathbf{B}\left(\tfrac{n}{2}, \tfrac{1}{2}\right)\tilde{a}^n - 2n^{1/n}\Lambda^{(n-1)/n}, \tag{37}$$

$$\tilde{P} \equiv \tilde{P}_{\mathrm{H}} + \tilde{P}_{\mathrm{a}} = \tfrac{1}{\pi}\mathbf{B}\left(\tfrac{1}{n} + 1, \tfrac{1}{2}\right)\tilde{a}^{n+1} - n^{2/n}\Lambda^{(n-2)/n}. \tag{38}$$

For $n = 2$, we have $\tilde{\delta}_{\mathrm{a}} = -\sqrt{8\Lambda} \to 0$ and $\tilde{P}_{\mathrm{a}} = -2$, which are the revised DMT results suggested by Maugis [2]. For convenience, we take the nomenclature of "DMT" and denote this limit case as DMT-n. The pull-off force is obtained at zero contact radius as

$$-\tilde{P}_{\mathrm{c}}^{\text{DMT-}n} = n^{2/n}\Lambda^{(n-2)/n}. \tag{39}$$

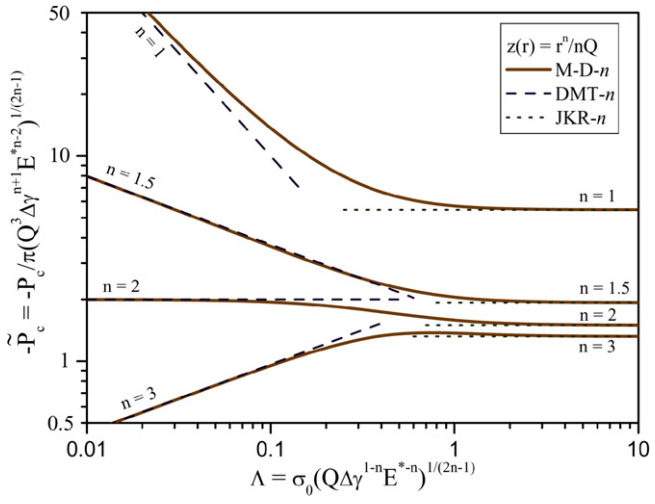

Fig. 2. Variation of the dimensionless pull-off force with the transition parameter for special cases of $n = 1$, 1.5, 2, and 3.

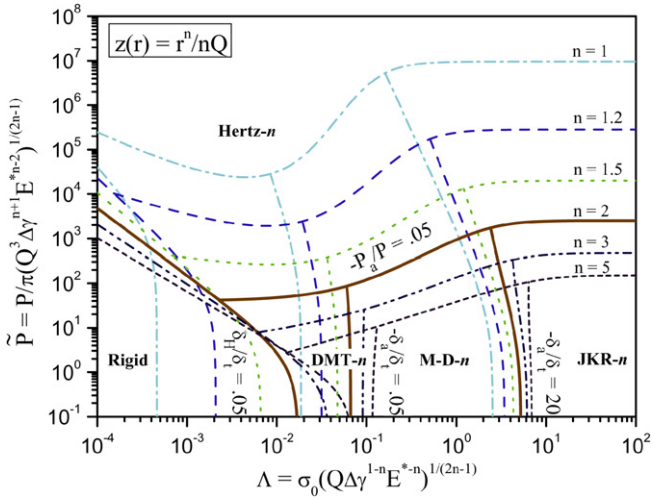

Fig. 3. The adhesion map for special cases $n = 1$, 1.2, 1.5, 2, 3, and 5.

For an arbitrary $n > 0$, as the dimensionless parameter Λ continuously changes from zero to infinity, a transition from DMT-n to JKR-n is apparent. So the dimensionless parameter Λ is named as a transition parameter. In Fig. 2, the variation of the dimensionless pull-off force $-\tilde{P}_c$ with the transition parameter Λ is plotted for several special cases, $n = 1$, 1.5, 2, and 3. At the small-Λ extreme, the dependence of the dimensionless pull-off force on the transition parameter Λ is negative for $n < 2$ and positive for $n > 2$. But at the large-Λ extreme, the dimensionless pull-off force $-\tilde{P}_c$ is independent of the transition parameter Λ for an arbitrary n. For $n = 1$, 1.5, 2, and 3, the limits of $-\tilde{P}_c$ at the large-Λ extreme are 5.471, 1.932, 1.5, and 1.320, respectively. Only for $n = 2$, the pull-off force $-P_c$ at both extremes is independent of the elastic modulus.

5. A three-dimensional adhesion map

It may be valuable to indicate the appropriate use of the contact models. For $n = 2$, as shown in Fig. 3 with a solid line, an adhesion map has been constructed by Johnson and Greenwood [18]. The thought can be extended to that of an arbitrary $n > 0$, based on the extended M–D model. For the Hertz-n zone, the boundary condition is $|P_a/P| < \xi$, where $\xi \ll 1$ is an arbitrarily chosen fraction. For the JKR-n zone, $|\delta_a/\delta_t| > \eta_1$, where $\eta_1 \gg 1$ and $\delta_t = \Delta\gamma/\sigma_0$ is the crack-opening displacement, while for the DMT-n zone, $|\delta_a/\delta_t| < \eta_2$, where $\eta_2 \ll 1$. For the rigid zone, the condition is $|\delta_H/\delta_t| < \zeta$, where $\zeta \ll 1$. It should be noticed that the rigid model has not been presented, but it will be discussed in Section 6.

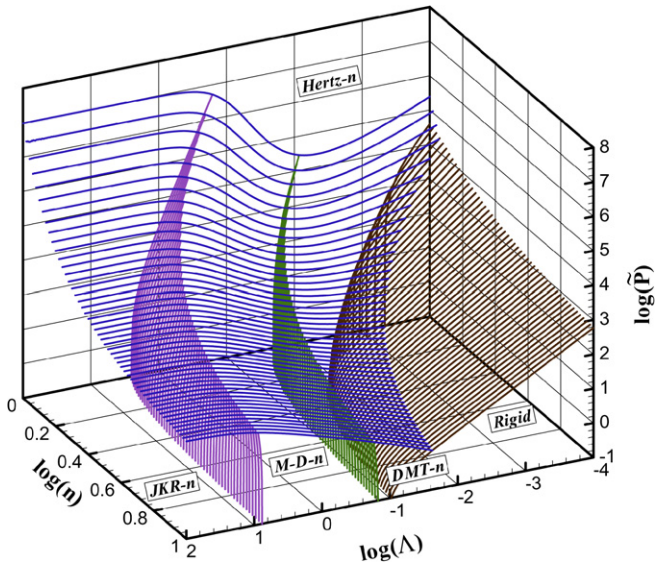

Fig. 4. The three-dimensional adhesion map.

The map with two coordinates, i.e., a transition parameter Λ and a dimensionless load $\tilde{P}$, is divided into five zones corresponding to the appropriate use of the Hertz-n, JKR-n, DMT-n, M–D–n, and rigid models. For the same numbers ($\xi = 0.05$, $\eta_1 = 20$, $\eta_2 = 0.05$, and $\zeta = 0.05$) as those chosen by Johnson and Greenwood [18], several special cases, i.e., $n = 1$, 1.2, 1.5, 3, and 5, are also plotted in Fig. 3. For an arbitrary $n > 0$, we extend the adhesion map to a three-dimensional one in Fig. 4 with an additional coordinate of the shape index n.

6. Matching a specific interaction

In this section, using the Dugdale approximation to match a specific interaction is discussed. For the adhesive contact of spheres, the step cohesive stress σ_0 was chosen to be the theoretical stress σ_{th} to match the Lennard-Jones potential [2]. It is somewhat arbitrary [18], but no other suggestion is found in the literature. Here, we propose an alternative one.

As the common one, we first consider the case of the Lennard-Jones potential,

$$p^*(h) = \frac{8\Delta\gamma}{3z_0}\left[(h/z_0)^{-9} - (h/z_0)^{-3}\right], \tag{40}$$

where h is the local separation, which is related to the gap by $h(r) = z_0 + [w(r/a)]$. Based on this interaction, the FSCM can be performed to obtain the load–displacement curves [9,10, 13–17]. A numerical method of iteration is used with several improvements, a variable-spacing technology, a central sepa-

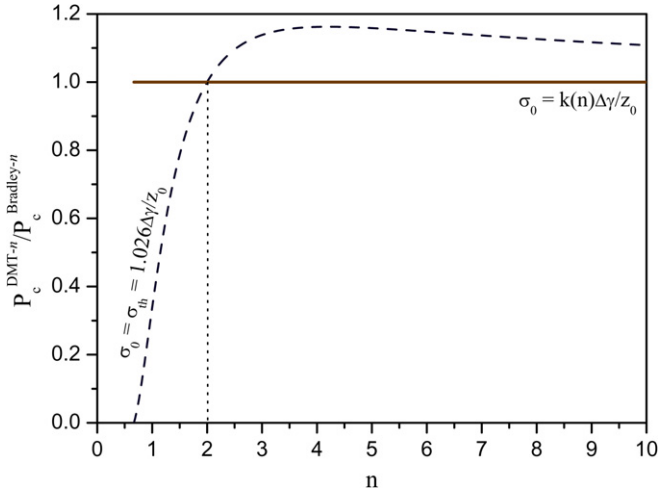

Fig. 5. A comparison of the DMT-n and Bradley-n pull-off forces.

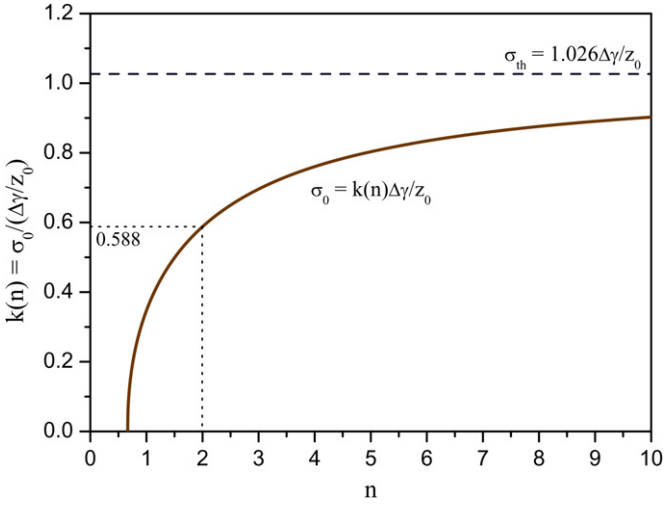

Fig. 6. The coefficient $k(n)$ involved in the Dugdale approximation to match the Lennard-Jones potential.

ration control, a Newton–Raphson method of iterations, and a Riemann–Stieltjes integral, to avoid the singularity pointed out by Greenwood [15]. For an arbitrary $n > 2/3$, it is found that there is an extended MYD transition from Bradley-n (see Appendix A) to JKR-n, varying with an extended Tabor number defined as

$$\mu \equiv \left(Q\Delta\gamma^n/E^{*n}z_0^{2n-1}\right)^{1/(2n-1)}. \tag{41}$$

The Bradley-n pull-off force is

$$-P_c^{\text{Bradley-}n} = \pi\phi(n)(nQz_0)^{2/n}(\Delta\gamma/z_0) \tag{42}$$

(see Eq. (A.5) for $\alpha = 9$ and $\beta = 3$), where

$$\phi(n) = \frac{32}{9n-2}\mathbf{B}\left(3-\tfrac{2}{n},\tfrac{2}{n}\right)\left(168\mathbf{B}\left(4-\tfrac{2}{n},6\right)\right)^{(3n-2)/6n}. \tag{43}$$

The JKR-n pull-off force is given in Eq. (35).

In Section 4, a transition from DMT-n to JKR-n is mentioned in the M–D–n model. Since the DMT-n model is an elastic contact one, this transition should be a part of the extended MYD transition. When the contact radius is zero, the DMT-n model does not have any elastic deformation, so it should be identical with the Bradley-n model. For $n = 2$, it is well known that the DMT and Bradley pull-off forces are both $2\pi R\Delta\gamma$, which was usually used without discrimination in the literature. For an arbitrary n, the DMT-n and Bradley-n pull-off forces are presented in Eqs. (39) and (42), respectively, so their ratio can be derived as

$$\frac{P_c^{\text{DMT-}n}}{P_c^{\text{Bradley-}n}} = \frac{1}{\phi(n)}\left(\frac{\sigma_0}{\Delta\gamma/z_0}\right)^{(n-2)/n}. \tag{44}$$

For $n = 2$, we have $\phi(2) = 1$ and $P_c^{\text{DMT-}n}/P_c^{\text{Bradley-}n} = 1$ for arbitrary σ_0. It seems that there is no unitary value for the stress σ_0 in this case. A suggestion presented by Maugis [2] for the stress σ_0 is the theoretical stress σ_{th}. No evidence has been shown that this selection is better than anything else. For other n, we will find that this selection is not wise. As clearly shown in Fig. 5 with the dashed line ($\sigma_0 = \sigma_{\text{th}}$), the value of $P_c^{\text{DMT-}n}/P_c^{\text{Bradley-}n}$ increases from zero at $n = 2/3$ to a maximum of 1.162 at $n = 4.210$ through one at $n = 2$, and then decreases with further increase of n to approach a limit of one at $n = \infty$.

For an arbitrary $n > 0$, in order to keep

$$-P_c^{\text{DMT-}n} = -P_c^{\text{Bradley-}n} \tag{45}$$

(Fig. 5 with solid line), we should have

$$\sigma_0 = k(n)\Delta\gamma/z_0, \tag{46}$$

where the coefficient $k(n)$ is defined as

$$k(n) = \left(\phi(n)\right)^{n/(n-2)}, \tag{47}$$

which is plotted in Fig. 6 with the solid line. It is transparent that an exclusive value for the stress σ_0 is required for an arbitrary n. The coefficient $k(n)$ increases with the increase of n. When $n \to \infty$, it approaches its maximum 1.026, which corresponds to the theoretical stress σ_{th}, as plotted in Fig. 6 with the dashed line. When $n = 1$, 1.5, 2, and 3, we have $k(n) = 0.347$, 0.499, 0.588, and 0.696, respectively. It should be noted that the value of $k(n)$ for $n = 2$ is derived by calculating the limit, and its exact form is

$$\lim_{n\to 2} k(n) = \exp(-223/420) \doteq 0.588, \tag{48}$$

which can be directly obtained with the aid of mathematical software. Hence, our alternative suggestion for the stress σ_0 in the case of $n = 2$ is $0.588\Delta\gamma/z_0$ ($\doteq$ ~~0.603~~σ_{th}). A comparison of the pull-off forces determined from the models is carried out for $n = 2$, as shown in Fig. 7. The pull-off forces of the M–D model using the stress σ_0 suggested by us ($\sigma_0 = 0.588\Delta\gamma/z_0$) and by Maugis ($\sigma_0 = 1.026\Delta\gamma/z_0$) are plotted. As is well known, the pull-off force of the M–D model with $\sigma_0 = 1.026\Delta\gamma/z_0$ is smaller than that of the FSCM for the moderate value of the Tabor number μ. It is surprising to find that the result by our suggestion is so close to the FSCM pull-off force, i.e., the MYD transition. This improvement is comprehensive. For example, in the case of $\mu = 1$ shown in Fig. 8, the load–displacement curve of the M–D model with $\sigma_0 = 0.588\Delta\gamma/z_0$ (corresponding to $\Lambda = 0.588\mu$, i.e., $\lambda = 1.127\Lambda = 0.663\mu$) is closer to that of

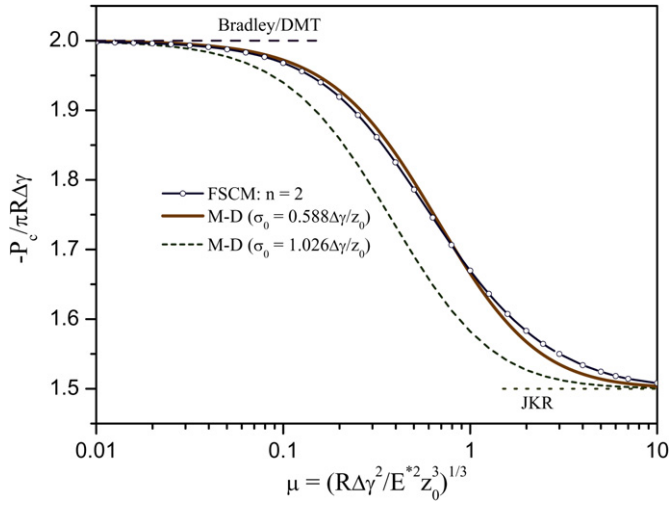

Fig. 7. Variation of the pull-off force with the Tabor number for the special case of $n = 2$.

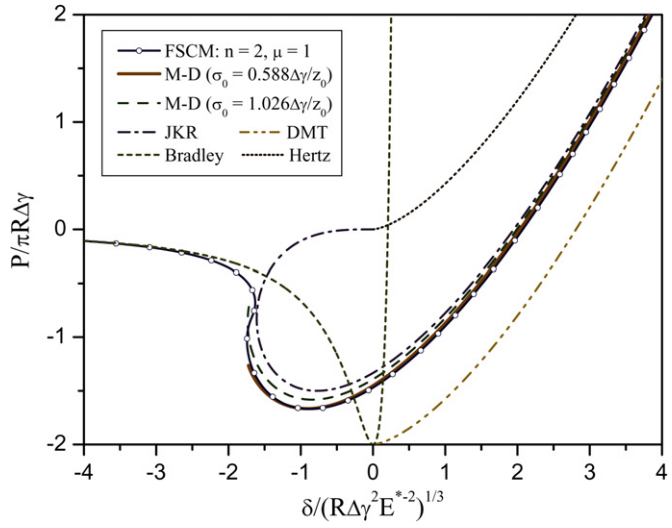

Fig. 8. Load–displacement curves for the special case of $n = 2$ and $\mu = 1$.

the FSCM than that of the M–D model with $\sigma_0 = 1.026\Delta\gamma/z_0$ (corresponding to $\lambda = 1.157\mu$). A more extensive comparison of the pull-off forces determined from the models is carried out for $n = 1$, 1.5, 2, and 3, as shown in Fig. 9, in which the dimensionless pull-off force is defined as

$$-\bar{P}_c \equiv -P_c/\pi\Delta\gamma Q^{2/n} z_0^{(2-n)/n}. \tag{49}$$

For $n = 1$, 1.5, 2, and 3, our suggestions for $k(n)$ are 0.347, 0.499, 0.588, and 0.696, which correspond to $\Lambda = 0.347\mu$, 0.499μ, 0.588μ, and 0.696μ, respectively. The figure shows that the pull-off forces of the M–D–n model are well agreeable with those of the FSCM. Although our suggestion of the identical pull-off force is only for the rigid limit, a good agreement over the whole transition is found.

For a more general relationship of the Lennard-Jones potential [10],

$$p^*(h) = \frac{(\alpha-1)(\beta-1)\Delta\gamma}{(\alpha-\beta)z_0}\left[(h/z_0)^{-\alpha} - (h/z_0)^{-\beta}\right],$$

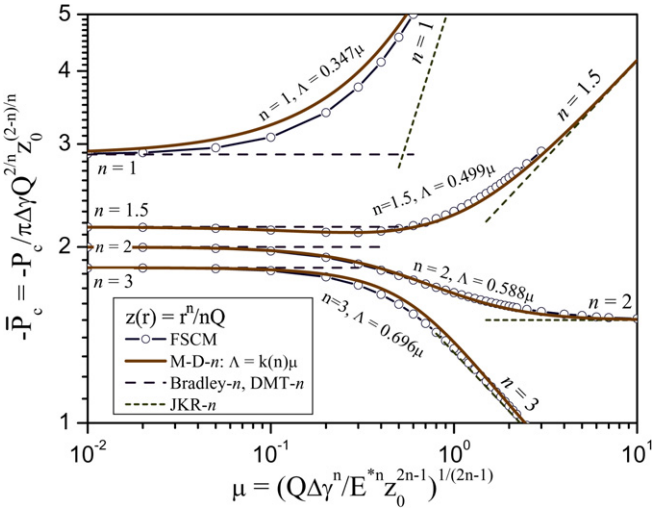

Fig. 9. Variation of the pull-off force with the Tabor number for $n = 1$, 1.5, 2, and 3.

$$\alpha > \beta > 1, \tag{50}$$

one may have the pull-off force at the rigid limit in Eq. (A.5), and then have Eq. (46) with the coefficient $k(n)$ in the more general form

$$k(n;\alpha,\beta) = \left[\frac{2(\alpha-1)(\beta-1)}{(\alpha n-2)}\mathbf{B}\left(\beta-\tfrac{2}{n},\tfrac{2}{n}\right) \times \left(\frac{\mathbf{B}(\beta+1-\frac{2}{n},\alpha-\beta)}{\mathbf{B}(\beta,\alpha-\beta)}\right)^{(\beta n-2)/(\alpha-\beta)n}\right]^{n/(n-2)}, \tag{51}$$

where $n > 2/\beta$. It is worth presenting the special cases of $n = 1$, 2, and ∞,

$$\lim_{n\to1} k(n;\alpha,\beta) = \frac{(\alpha-2)(\beta-2)}{2(\alpha-1)}\left(\frac{\beta-1}{\alpha-1}\right)^{(\beta-2)/(\alpha-\beta)}, \tag{52}$$

$$\lim_{n\to2} k(n;\alpha,\beta) = \exp\left[\frac{\alpha-1}{\alpha-\beta}\left(\gamma+\psi_0(\beta)\right) - \frac{\beta-1}{\alpha-\beta}\left(\gamma+\psi_0(\alpha)\right) - \frac{\alpha\beta-1}{(\alpha-1)(\beta-1)}\right], \tag{53}$$

$$\lim_{n\to\infty} k(n;\alpha,\beta) = (\alpha-1)(\beta-1)(\beta^\beta/\alpha^\alpha)^{1/(\alpha-\beta)}, \tag{54}$$

where γ is the Euler constant and $\psi_0(\alpha) \equiv \mathbf{\Gamma}'(\alpha)/\mathbf{\Gamma}(\alpha)$ is the digamma function, with $\mathbf{\Gamma}(\alpha)$ being the Euler gamma function. If α is an integer, then $\psi_0(\alpha) = -\gamma + \mathbf{H}_{\alpha-1}$, where $\mathbf{H}_{\alpha-1}$ is the harmonic number.

With the relation of *the identical pull-off force at the rigid limit*, we can use the Dugdale approximation to nearly match a specific interaction. Its validity can be verified by an extensive comparison with that of FSCM. This supplementary relation to the Maugis model may make it more efficient to fit data in practice.

7. Conclusions

In this paper, the Maugis model of the frictionless adhesive contact of spheres is extended to contact of arbitrary axisym-

metric elastic objects with an arbitrary surface adhesive interaction, named the generalized Maugis model. Applying this model to the power-law axisymmetric objects and using the Dugdale approximation, we obtain an extended M–D model, which can be solved easily with a numerical calculation. Under some limit conditions, it can even be simplified to a completely analytic form. At the small-Λ extreme, it is simplified to the extended DMT model. It should be noticed that the "DMT" nomenclature is referred to the revised DMT model but not the original or improved one. At the large-Λ extreme, the extended M–D model is simplified to the extended JKR model. A continuous transition from the extended DMT model to the extended JKR model is found for an arbitrary shape index. Based on the extended M–D model, a three-dimensional adhesion map is constructed with the dimensionless coordinates of the transition parameter Λ, the dimensionless load $\tilde{P}$, and the shape index n.

Using the Dugdale approximation to match a specific interaction, for example the Lennard-Jones potential, is discussed. It is found that the suggestion of the theoretical stress $\sigma_{\text{th}} \doteq 1.026\Delta\gamma/z_0$ for the step cohesive stress σ_0 in Ref. [2] is too large for an arbitrary $n < \infty$. An alternative one, $k(n)\Delta\gamma/z_0$, where $k(n)$ is a coefficient related to the shape index n, is determined from the requirement of identical pull-off force at the rigid limit. For the limit case of $n = 2$, the stress σ_0 is $0.588\Delta\gamma/z_0$ ($\doteq 0.603\sigma_{\text{th}}$). This result shows better agreement with the MYD transition than that of $1.026\Delta\gamma/z_0$. The stress σ_0 for the Dugdale approximation to match the general Lennard-Jones potential is also presented.

Two independent relations, the condition of no singularity and the Griffith relation, employed by Maugis lead the elastic adhesive contact problem to an analytic model. In this paper, a supplementary relation of the identical pull-off force at the rigid limit is employed to make the approximate model to match the exact one. The model involving these three relations is simple in numerical calculations and efficient for fitting data in practice.

Acknowledgment

This work is supported by the Graduate Innovation Fund of USTC (KD2004036).

Appendix A. The Bradley-*n* pull-off force

The applied load is derived by integrating the surface interaction

$$P = \int_0^\infty p^*\big(h(r)\big)\,2\pi r\,dr. \tag{A.1}$$

For power-law axisymmetric objects, if the material is rigid, the surface separation is given by

$$h(r) = z_0 - \delta + r^n/nQ. \tag{A.2}$$

Thus, we have

$$n^{(2-n)/n}Q^{2/n}\big(h(r) - z_0 + \delta\big)^{(2-n)/n}\,dh(r) = r\,dr. \tag{A.3}$$

Considering the surface interaction in the general Lennard-Jones potential, Eq. (50), we immediately obtain the Bradley-*n* equation,

$$P = \frac{2\pi(\alpha-1)(\beta-1)\Delta\gamma}{(\alpha-\beta)nz_0}(nQz_0)^{2/n}\Big[\mathbf{B}\big(\alpha-\tfrac{2}{n},\tfrac{2}{n}\big) \times (1-\delta/z_0)^{-\alpha-2/n} - \mathbf{B}\big(\beta-\tfrac{2}{n},\tfrac{2}{n}\big)(1-\delta/z_0)^{-\beta-2/n}\Big], \tag{A.4}$$

and its pull-off force,

$$-P_{\text{c}}^{\text{Bradley-}n} = \pi\phi(n;\alpha,\beta)(nQz_0)^{2/n}(\Delta\gamma/z_0), \tag{A.5}$$

where

$$\phi(n;\alpha,\beta) = \frac{2(\alpha-1)(\beta-1)}{\alpha n-2}\mathbf{B}\big(\beta-\tfrac{2}{n},\tfrac{2}{n}\big) \times \left(\frac{\mathbf{B}(\beta+1-\frac{2}{n},\alpha-\beta)}{\mathbf{B}(\beta,\alpha-\beta)}\right)^{(\beta n-2)/(\alpha-\beta)n}. \tag{A.6}$$

References

[1] D. Maugis, Contact, Adhesion and Rupture of Elastic Solids, Springer-Verlag, Berlin, 2000.
[2] D. Maugis, J. Colloid Interface Sci. 13 (1992) 243.
[3] K.L. Johnson, K. Kendall, A.D. Roberts, Proc. R. Soc. London Ser. A 324 (1971) 301.
[4] D. Maugis, M. Barquins, J. Phys. D 11 (1978) 1989.
[5] B.V. Derjaguin, V.M. Muller, Y.P. Toporov, J. Colloid Interface Sci. 53 (1975) 314.
[6] V.M. Muller, B.V. Derjaguin, Y.P. Toporov, Colloids Surf. 7 (1983) 251.
[7] M.D. Pashley, Colloids Surf. 12 (1984) 69.
[8] D. Tabor, J. Colloid Interface Sci. 58 (1977) 1.
[9] V.M. Muller, V.S. Yushchenko, B.V. Derjaguin, J. Colloid Interface Sci. 77 (1980) 91.
[10] V.M. Muller, V.S. Yushchenko, B.V. Derjaguin, J. Colloid Interface Sci. 92 (1983) 92.
[11] B.D. Hughes, L.R. White, J. Mech. Appl. Math. 32 (1979) 445.
[12] B.D. Hughes, L.R. White, J. Chem. Soc. Faraday Trans. 176 (1980) 963.
[13] P. Attard, J.L. Parker, Phys. Rev. A 46 (1992) 7959.
[14] P. Attard, J. Phys. Chem. B 104 (2000) 10635.
[15] J.A. Greenwood, Proc. R. Soc. London Ser. A 453 (1997) 1277.
[16] J.Q. Feng, Colloids Surf. A 172 (2000) 175.
[17] J.Q. Feng, J. Colloid Interface Sci. 238 (2001) 318.
[18] K.L. Johnson, J.A. Greenwood, J. Colloid Interface Sci. 192 (1997) 326.
[19] E. Barthel, J. Colloid Interface Sci. 200 (1998) 7.
[20] R. Carpick, N. Agrait, D. Ogletree, M. Salmeron, J. Vac. Sci. Technol. B 14 (1996) 1289.
[21] R. Carpick, N. Agrait, D. Ogletree, M. Salmeron, J. Vac. Sci. Technol. B 14 (1996) 2772.
[22] F.M. Borodich, B.A. Galanov, in: International Congress of Theoretical and Applied Mechanics (ICTAM), Warsaw, Poland, 2004.
[23] R. Spolenak, S. Gorb, H.J. Gao, E. Arzt, Proc. R. Soc. London Ser. A 461 (2005) 305.
[24] I.G. Goryacheva, Y.Y. Makhovskaya, J. Appl. Math. Mech. 65 (2001) 273.
[25] I.N. Sneddon, Int. J. Eng. Sci. 3 (1965) 47.
[26] M. Lowengrub, I.N. Sneddon, Int. J. Eng. Sci. 3 (1965) 451.
[27] K. Kendall, J. Phys. D 4 (1971) 1186.
[28] D. Maugis, M. Barquins, J. Phys. Lett. 42 (1981) L95.